On the relationship between pump chirp and single-photon chirp in spontaneous parametric downconversion

Xochitl Sanchez-Lozano[1]**, Alfred B U'Ren**[2] **and Jose Luis Lucio**[1]

[1] División de Ciencias e Ingenierías, Universidad de Guanajuato, PO Box E-143, 37150 León
Guanajuato, Mexico
[2] Instituto de Ciencias Nucleares, Universidad Nacional Autónoma de México, Apartado Postal 70-543,
04510 DF, Mexico

Abstract
We study the chronocyclic character, i.e. the joint temporal and spectral properties, of the
single-photon constituents of photon pairs generated by spontaneous parametric
downconversion. In particular we study how single-photon properties, including purity and
single-photon chirp, depend on photon-pair properties, including the type of signal–idler
spectral and correlations and the level of pump chirp.

(Some figures may appear in colour only in the online journal)

---

1. Introduction

Single photons constitute the most fundamental building block of optical fields. Single photons are often described in terms of a single optical mode described by an annihilation operator $\hat{a}$, i.e. as $\hat{a}^{\dagger}|0\rangle$, where $|0\rangle$ is the vacuum. However, single photons emitted through actual physical processes are, of course, wavepackets involving different optical frequencies as well as different directions of propagation. A complete understanding of single photons emitted under realistic conditions therefore requires an in-depth study of their multi-modal richness.

In this paper we concentrate our study on single photons derived from photon pairs emitted through the process of spontaneous parametric downconversion (SPDC) in second-order nonlinear crystals. Likewise, we focus on the spectral degree of freedom in the SPDC photon pairs. The process of SPDC can be extremely versatile as the basis for photon-pair source design; indeed, a careful selection of the source configuration leads to the ability to widely select the properties of the emitted photon pairs. Thus, for example, photon-pair sources exhibiting entanglement in discrete photonic degrees of freedom (such as polarization [1, 2] and orbital angular momentum [3]), and alternatively exhibiting entanglement in continuous degrees of freedom [4, 5] (such

as frequency/time [6], transverse momentum/position [7]), have been demonstrated. In the specific case of the spectral degree of freedom, photon-pair sources have been designed and demonstrated with a large range of behaviors in terms of the emission bandwidth (ranging from tens of MHz [8] to hundreds of THz [10]) and in terms of the degree of the entanglement (ranging from factorable [9] to highly entangled [10]).

The detection of one of the two photons in a given SPDC pair can herald the presence of its conjugate, an approach often used as the basis for single-photon sources [11, 12]. Heralded single photons have been characterized in previous works, for example through a measurement of the corresponding Wigner function in the phase space formed by the position and momentum electric field quadratures [13, 14]. In this paper we are primarily interested in studying how the spatial and temporal properties of the pump translate into specific properties of the constituent single photons, in particular in the time–frequency degree of freedom. Indeed, in a recent work from our group, we have shown that pump chirp may be used in order to control effectively the degree of entanglement in SPDC photon pairs, and consequently control the purity of the constituent single photons [15]. We have shown that, if the source is designed so that in the absence of pump chirp photon pairs are factorable, or equivalently so that the

constituent single photons are pure [16], an arbitrary degree of photon-pair entanglement, or single-photon purity, can be attained by varying the level of pump chirp.

Besides the single-photon purity, in this paper we are also interested in the chronocyclic character, i.e. in the joint spectral–temporal properties, of the single photons. Specifically, we are interested in studying how the chronocyclic character of the pulse train associated with a broadband pump defines the chronocyclic character of the emitted single photons. While this is interesting from a fundamental physics perspective, it is also important in the context of quantum information processing (QIP) applications which rely on single photons. Knowledge of the full multi-mode structure of single photons is essential for the correct design of specific QIP implementations. Indeed, an understanding of, and the ability to control, these chronocyclic properties are crucial for the correct mode matching of single photons to other photonic modes in interferometric arrangements. For example, both Hong–Ou–Mandel interference of single photons from distinct sources, and homodyning of single photons with a coherent state, depend crucially on the single-photon chronocyclic character. Therefore, it is important to understand how pump chirp, used as a tool for tailoring the level of spectral entanglement present in SPDC photon pairs, also determines the chronocyclic character of the single photons which constitute each pair.

An ideal framework in which to study the single-photon joint spectral–temporal properties is the single-photon chronocyclic Wigner function (CWF). In this paper, we study the relationships between the single-photon spectral density matrix, the first-order degree of spectral and temporal coherence, and the single-photon CWF. We study in particular how the type of spectral correlations in the SPDC photon pairs, together with the level of pump chirp, determine on the one hand the purity and, on the other hand, the presence of spectral–temporal correlations, or chirp, in the single photons.

2. SPDC photon pairs, and their constituent single photons

In the spontaneous parametric downconversion process (SPDC) an optical crystal with a second-order nonlinearity is illuminated by a laser pump beam. Individual photons from the pump beam may then be annihilated, leading to the emission of photon pairs, where the two photons in a given pair are typically referred to as signal and idler. These photon pairs may be entangled in any of the photonic degrees of freedom, including polarization, time–frequency and transverse position–momentum. In this paper we concentrate on the spectral degree of freedom; specifically, we assume that appropriate spatial filtering on the signal and idler modes is used so that only specific directions of propagation are retained.

Following a standard perturbative approach, the two-photon state for the SPDC process can be written as $|\Psi\rangle = |0\rangle + \eta|\Psi_2\rangle$, in terms of the two-photon component of the state $|\Psi_2\rangle$

$$|\Psi_2\rangle = \int d\omega_s \int d\omega_i f(\omega_s, \omega_i)|\omega_s\rangle|\omega_i\rangle, \qquad (1)$$

where η is related to the conversion efficiency, $f(\omega_s, \omega_i)$ is the joint spectral amplitude (JSA) function, $|\omega_\mu\rangle = \hat{a}_\mu^\dagger(\omega)|0\rangle$ with $\mu = i, s$ and $|0\rangle$ represents the vacuum state.

The focus of this paper is on the properties of the single photons which constitute each of the SPDC pairs. Specifically, we are interested in studying how the single-photon properties are determined by the photon-pair properties. Each of the single photons in a given pair is completely characterized by its respective density operator. For the specific case of the signal mode, the density operator $\hat{\rho}_s$ can be written as

$$\hat{\rho}_s = \text{Tr}_i(|\Psi\rangle\langle\Psi|), \qquad (2)$$

where Tr_i represents a partial trace over the idler mode. In terms of the JSA, the reduced density operator can be expressed through its matrix elements as

$$\rho_s(\omega_1, \omega_2) \equiv \langle\omega_1|\hat{\rho}_s|\omega_2\rangle$$
$$= \int d\omega_0 f(\omega_1, \omega_0)f^*(\omega_2, \omega_0). \qquad (3)$$

The density matrix $\rho_s(\omega_1, \omega_2)$ fully characterizes the signal-mode single photons. Note that the normalization condition on the density operator $\text{Tr}(\hat{\rho}_s) = 1$ is equivalent to the normalization condition $\int d\omega_s \int d\omega_i |f(\omega_s, \omega_i)|^2 = 1$ for the JSA function. For what follows, it is convenient to write down the density matrix expressed in terms of diagonal ω and off-diagonal ω' frequency components, $\rho^D(\omega, \omega')$, where ω and ω' are related to ω_1 and ω_2 through $\omega_1 = \omega + \omega'/2$ and $\omega_2 = \omega - \omega'/2$:

$$\rho_s^D(\omega, \omega') = \rho_s\left(\omega + \frac{\omega'}{2}, \omega - \frac{\omega'}{2}\right). \qquad (4)$$

An important property of the single photons is their purity, quantified by

$$p \equiv \text{Tr}(\hat{\rho}^2) = \int d\omega_1 \int d\omega_2 |\rho_s(\omega_1, \omega_2)|^2. \qquad (5)$$

Aside from the purity, in this paper we are interested in the spectral and temporal properties of the single photons. The Wigner distribution function applied to the time-varying electric field provides a mathematical tool which can represent classical light pulses in chronocyclic, i.e. in time–frequency, space [17]. This leads to a representation that shows intertwined temporal and spectral effects, aiding a better comprehension of certain optical phenomena. In the realm of quantum optics, it is convenient to study the temporal and spectral properties of single photons through the single-photon chronocyclic Wigner function [18]. Indeed, while the density matrix contains complete information about the single photons, in this paper we also use the single-photon chronocyclic function (CWF) $W(\omega, t)$, because this leads to a better direct appreciation of the temporal, as well as spectral, properties of the single photons. In particular, phase information which is absent from the absolute value of the density matrix $|\rho_s(\omega_1, \omega_2)|$ appears naturally in the real-valued CWF. Certain spectral–temporal properties such as single-photon chirp become more directly apparent in the chronocyclic domain.

The density matrix $\rho(\omega_1, \omega_2)$ and the chronocyclic Wigner function $W(\omega, t)$ are related to each other through a Fourier transform, as follows:

$$W(\omega, t) = \frac{1}{2\pi} \int d\omega' \, \rho_s^D(\omega, \omega') e^{-i\omega' t}. \quad (6)$$

Or, conversely,

$$\rho_s^D(\omega, \omega') = \int dt \, W(\omega, t) e^{i\omega' t}. \quad (7)$$

It is known that integration of the CWF over the time variable yields the single-photon spectral intensity or single-photon spectrum (SPS) $I_\omega(\omega)$. Thus, we can show that the SPS is closely related to the diagonal elements of the density matrix, i.e.

$$I_\omega(\omega) \equiv \int dt \, W(\omega, t) = \rho_s(\omega, \omega) = \rho_s^D(\omega, 0). \quad (8)$$

The function $\rho_s(\omega, \omega)$ is then related to the 'population of each single-photon spectral component', in other words to the relative spectral intensity at each of the spectral components. Normalization of $I_\omega(\omega)$, so that $\int d\omega \, I_\omega(\omega) = 1$ is guaranteed by the normalization of the density matrix, i.e. $\text{Tr}(\rho_s) = 1$. The off-diagonal elements, or 'coherences between different spectral components', which occur for $\omega' \neq 0$, then can have non-zero values for pure states and vanish for highly impure states. In fact, the interpretation of the off-diagonal elements as coherences may be made direct by observing that there is a simple relationship between the first degree of spectral coherence $S(\omega_1, \omega_2)$ between two frequencies ω_1 and ω_2 and the density matrix $\rho(\omega_1, \omega_2)$. $S(\omega_1, \omega_2)$ may be defined as follows [19]:

$$S(\omega_1, \omega_2) \equiv \text{Tr}[\hat{\rho}_s a^\dagger(\omega_1) a(\omega_2)]. \quad (9)$$

It is then a simple matter to show that

$$S(\omega_1, \omega_2) = \rho^*(\omega_1, \omega_2). \quad (10)$$

Alternatively, we may choose to study the coherence between two different times. In this case, we define the first degree of coherence $\Gamma(t_1, t_2)$ between two different times t_1 and t_2. In terms of the time-domain annihilation operator $\tilde{a}(t) = \int d\omega \, a(\omega) e^{-i\omega t}$, $\Gamma(t_1, t_2)$ may be defined as

$$\Gamma(t_1, t_2) \equiv \text{Tr}[\hat{\rho}_s \tilde{a}^\dagger(t_1) \tilde{a}(t_2)]. \quad (11)$$

It can then be shown that $\Gamma(t_1, t_2)$ may be expressed in terms of the density matrix $\rho^D(\omega, \omega')$ as

$$\Gamma(t_1, t_2) = \int d\omega \int d\omega' \, \rho^D(\omega, \omega') e^{-i\frac{\omega'}{2}(t_1 + t_2)} e^{i\omega(t_1 - t_2)}, \quad (12)$$

or alternatively we may also relate $\Gamma(t_1, t_2)$ to the CWF $W(\omega, t)$ through

$$\Gamma\left(t + \frac{t'}{2}, t - \frac{t'}{2}\right) = 2\pi \int d\omega \, W(\omega, t) e^{i\omega t'}, \quad (13)$$

which corresponds to a form of the Wiener–Khintchine theorem for single photons [19].

Thus, the Fourier transform of $\rho^D(\omega, \omega')$ with respect to the anti-diagonal frequency component ω' yields the

Wigner function $W(\omega, t)$, while the Fourier transform of the Wigner function with respect to the diagonal frequency component yields the first-order temporal coherence function $\Gamma(t + t'/2, t - t'/2)$. Note that if we define a density matrix in the temporal domain $\rho_s^T(t_1, t_2) \equiv \langle t_1 | \hat{\rho}_s | t_2 \rangle$, in terms of $|t\rangle \equiv \tilde{a}^\dagger(t) |0\rangle$, it is straightforward to show that $\rho_s^T(t_1, t_2) = \Gamma^*(t_1, t_2)$, a relationship which mirrors its counterpart in the spectral domain. Inverting equation (13) leads to a relationship between $\rho^D(\omega, \omega')$ and $W(\omega, t)$, where the roles of time and frequency are reversed with respect to those in equation (6), i.e.

$$W(\omega, t) = \frac{1}{4\pi^2} \int dt' \, \rho_s^T\left(t - \frac{t'}{2}, t + \frac{t'}{2}\right) e^{-i\omega t'}, \quad (14)$$

which could be regarded as an alternative definition for the CWF.

Returning to the spectral domain, let us examine the conditions for the off-diagonal single-photon density matrix elements to be non-zero. In terms of ω and ω', the density matrix is given by the integral over ω_0 of $f(\omega + \omega'/2, \omega_0) f^*(\omega - \omega'/2, \omega_0)$. For a given pair of signal and idler frequencies $\omega_s = \omega$ and $\omega_i = \omega_0$, for this integrand to be non-zero, clearly the JSA function must not vanish at the symmetrically displaced pair of signal-mode frequencies $\omega + \omega'/2$ and $\omega - \omega'/2$. Indeed, for a given ω and ω_0 the width in the frequency variable ω' of the integrand is closely related to the width of the JSA function along the signal-mode frequency variable. Note that, if a one-to-one correspondence exists between the signal and idler frequencies, then this resulting width is zero and the integrand above will be proportional to $\delta(\omega')$. Thus, a first condition for the off-diagonal signal-mode single-photon density matrix elements to be non-zero is that each idler frequency corresponds to a spread of signal frequencies rather than to a single signal frequency, i.e. that a strict correlation between signal and idler frequencies does not exist. Note that, while a one-to-one correspondence in the signal and idler frequencies is consistent with maximal spectral entanglement, the correspondence of each idler frequency to a spread of signal frequencies is consistent with non-maximal spectral entanglement.

Even if each $\omega_i = \omega_0$ frequency corresponds to a spread of signal frequencies, the integration over the idler frequency ω_0 implies that the single-photon density matrix may still exhibit vanishing off-diagonal elements. Indeed, if the integrand is oscillatory in the variable ω_0, integration may lead to averaging and therefore to small or vanishing values. One way in which this may occur is in the case where the pump mode is chirped. In the specific case of a quadratic chirp, quantified by the parameter β, the JSA becomes

$$f(\omega_s, \omega_i) = f_0(\omega_s, \omega_i) \exp[i\beta (\omega_s + \omega_i - \omega_p^0)^2], \quad (15)$$

where $f_0(\omega_s, \omega_i)$ represents the unchirped JSA. In this case the density matrix becomes

$$\rho_s^D(\omega, \omega') = e^{i2\beta\omega'(\omega - \omega_p^0)} \int d\omega_0 f_0\left(\omega + \frac{\omega'}{2}, \omega_0\right)$$

$$\times f_0^*\left(\omega - \frac{\omega'}{2}, \omega_0\right) e^{i2\beta\omega'\omega_0}. \quad (16)$$

For given non-zero ω' and β values, the phase term in the integrand leads to oscillations as ω_0 is varied, with an oscillation period given by $\pi/(\beta\omega')$. Thus, if the integration range for ω_0 is of the order of, or if it exceeds, this period, integration over ω_0 tends to make the off-diagonal elements vanish. A large chirp parameter β, or large ω' value (indicating matrix elements far from the diagonal), lead to a small oscillation period and thus favors small off-diagonal elements.

Thus, the existence of strong signal–idler correlations or the use of a chirped pump both lead to a small width of the density matrix $\rho_s^D(\omega, \omega')$ along ω', and therefore favor a diagonal density matrix structure. In the case of highly impure states, obtained through either of these two routes, the density matrix may be expressed as

$$\rho_s^D(\omega, \omega') = \frac{1}{\sqrt{\pi}\sigma'} I_\omega(\omega) e^{-\frac{\omega'^2}{\sigma'^2}} \qquad (17)$$

where σ' is a small quantity. For a strictly impure state with $\sigma' \to 0$ the CWF is then, according to the Fourier transform relationship of equation (6), time-independent, i.e.

$$W(\omega, t) \propto I_\omega(\omega). \qquad (18)$$

Thus, a perfectly impure state leads to a constant temporal intensity profile, or in other words to an infinite single-photon temporal duration. Also, note from equations (13) and (18) that such a perfectly impure state leads to a first-degree temporal coherence function of the following form:

$$\Gamma(t_1, t_2) \propto \int d\omega \, I_\omega(\omega) e^{i\omega(t_1-t_2)}. \qquad (19)$$

Note that the above $\Gamma(t_1, t_2)$ depends on the two arguments only through their difference. In other words, a perfectly impure single-photon state is statistically temporally stationary. In general terms, there is a link between the temporal duration of the signal photon and its degree of purity. In order to study this link, let us consider the temporal intensity profile $I_t(t)$ of the signal-mode single photon. This function is given by

$$I_t(t) \equiv \int d\omega \, W(\omega, t)$$
$$= \frac{1}{2\pi} \int d\omega' \int d\omega \, \rho_s^D(\omega, \omega') e^{-i\omega't}. \qquad (20)$$

Normalization of $I_t(t)$, i.e. $\int dt \, I_t(t) = 1$, is guaranteed by the normalization of the density matrix, i.e. $\text{Tr}(\hat{\rho}_s) = 1$. As is clear from equation (20), this temporal profile is given by the Fourier transform of the density matrix averaged over all ω values. For an increasingly impure single-photon state, leading to a density matrix with an increasingly diagonal structure, the width of the $\int d\omega \, \rho_s^D(\omega, \omega')$ function along ω' is reduced, leading to an increased signal-mode temporal duration as dictated by the Fourier transform relationship of equation (20). This is consistent with the analysis in [18] carried out in the context of the Gaussian approximation for the JSA, leading to the result $\delta t \delta\omega = 1/p$, where δt and $\delta\omega$ are the temporal duration and spectral width of the signal-mode single photon, respectively, and p is the single-photon purity. Thus, for example, as the pump chirp β is increased, while $\delta\omega$ (the width of the marginal distribution of the joint spectrum $|f(\omega_s, \omega_i)|^2$) remains fixed, since the two-photon state depends on β only through a phase, the temporal duration δt is increased, leading to an increased product $\delta t \delta\omega$, and consequently to a reduced purity p.

The relationship between photon-pair entanglement and single-photon purity is well understood. In fact, single-photon purity is simply the reciprocal of the Schmidt number K, which quantifies the degree of photon-pair entanglement. This underscores the importance of factorable states, with $K = 1$, which lead to pure states, with $p = 1$. Conversely, highly entangled photon pairs, with $K \to \infty$, lead to highly impure single photons with $p \to 0$ [16].

The joint spectral amplitude $f(\omega_s, \omega_i)$ can be written as follows:

$$f(\omega_s, \omega_i) = \phi(\omega_s, \omega_i)\alpha(\omega_s + \omega_i) e^{i\beta(\omega_s+\omega_i-\omega_p^0)^2}, \qquad (21)$$

in terms of the phasematching function (PMF) $\phi(\omega_s, \omega_i)$ which describes the optical properties of the nonlinear crystal, and the pump envelope function (PEF) $\alpha(\omega) e^{i\beta(\omega-\omega_p^0)^2}$ which explicitly includes a quadratic chirp phase. The PMF may be written as $\phi(\omega_s, \omega_i) = \text{sinc}[L\Delta k(\omega_s, \omega_i)/2]$, in terms of the crystal length L and of the phasemismatch $\Delta k(\omega_s, \omega_i) = k_p(\omega_s + \omega_i) - k_s(\omega_s) - k_i(\omega_i)$; here k_ν (with $\nu = $ p, s, i) represents the wavenumber for each of the pump (p), signal (s) and idler (i).

In order to facilitate the analysis below, it is helpful to rely on an analytical expression for the CWF. As discussed in [18], this can be achieved through two approximations: (i) expressing the JSA function entirely in terms of Gaussian functions and (ii) relying on a power series expansion, truncated at first order, of the Gaussian-approximated JSA argument. In this case, we can write the JSA function expressed in terms of detunings $\nu_{s,i} = \omega_{s,i} - \omega_{s,i}^0$ (where $\omega_{s,i}^0$ represent signal/idler central phasematched frequencies) as

$$f(\nu_s, \nu_i) = e^{-[X_{ss}^2\nu_s^2 + X_{ii}^2\nu_i^2 + 2(X_{si}^2-i\beta)\nu_s\nu_i]}. \qquad (22)$$

In equation (22) we have used the following definition, with $\lambda, \mu = $ s, i: $X_{\lambda\mu} \equiv \frac{1}{\sigma^2} + \frac{\gamma\tau_\lambda\tau_\mu}{4}$, in turn written in terms of the pump bandwidth σ, the pump chirp parameter β and parameter $\gamma = 0.193$ (related to the Gaussian approximation of the JSA, see [18]). This definition is also in terms of the signal/idler group velocity mismatch parameters τ_λ (with $\lambda = $ s, i) given in terms of the crystal length L as $\tau_\lambda = L(k_p' - k_\lambda')$; here, k' denotes the frequency derivative of the wavenumber associated with the each of the modes (p, s, i), evaluated at the respective central frequency.

Carrying out the corresponding integrations (equations (3) and (6)), we obtain the following expression for the CWF valid, for $\tau_s \neq \tau_i$:

$$W_s(\nu, t) = \frac{\sqrt{1-\mathscr{C}^2}}{\pi\,\Delta t\,\Delta\omega} e^{-\left(\frac{\nu}{\Delta\omega}\right)^2} e^{-\left(\frac{t}{\Delta t}\right)^2} e^{-2\mathscr{C}\left(\frac{\nu}{\Delta\omega}\right)\left(\frac{t}{\Delta t}\right)}. \qquad (23)$$

The parameters in equation (23) include a spectral width parameter $\Delta\omega$, its square given by

$$\Delta\omega^2 = \frac{\beta^2 + X_{ss}X_{ii}}{2[\beta^2(X_{ss} - 2X_{si} + X_{ii}) + X_{ss}(X_{ss}X_{ii} - X_{si}^2)]}, \quad (24)$$

a temporal width parameter Δt, its square given by

$$\Delta t^2 = \frac{2(\beta^2 + X_{ss}X_{ii})}{X_{ii}}, \quad (25)$$

and a single-photon chirp parameter $\mathscr{C}$ given by

$$\mathscr{C} = \frac{\beta(X_{ii} - X_{si})}{\sqrt{X_{ii}[\beta^2(X_{ss} - 2X_{si} + X_{ii}) + X_{ss}(X_{ss}X_{ii} - X_{si}^2)]}}. \quad (26)$$

When plotted in a normalized chronocyclic space $\{v/\Delta\omega, t/\Delta t\}$, the CWF has a circular shape for $\mathscr{C} = 0$ and becomes elongated diagonally for $\mathscr{C} \neq 0$. In particular, for $0 < \mathscr{C} < 1$ the distribution involves correlated frequencies and times, while for $-1 < \mathscr{C} < 0$ the distribution involves anti-correlated frequencies and times. For $|\mathscr{C}| = 1$, the distribution becomes infinitely elongated, indicating the maximum degree of single-photon chirp. Using the inequality $X_{si}^2 \leq X_{ss}X_{ii}$, which may be readily proved, it is straightforward to show that equation (26) indeed fulfills $|\mathscr{C}| \leq 1$.

In the limiting case where $\tau_s \to \tau_i$, corresponding to frequency anti-correlated photon pairs, $X_{si} \to X_{ss} = X_{ii}$ and it may be shown that $\Delta\omega \to \infty$ and $\mathscr{C} \to 0$. This resulting infinite spectral width appears because for anti-correlated photon pairs the phasematching function and the pump envelope function have the same orientation in $\{\omega_s, \omega_i\}$ space, and within the linear approximation of the phasemismatch used for the analytical expression of the CWF (equations (23)–(26)), the curvature of the phasematching function is suppressed. In a realistic, i.e. unapproximated, situation, the non-zero curvature leads to a finite (but large) spectral width.

As is evident from equation (26), in general in the absence of pump chirp, the signal-mode single photons are likewise unchirped. The presence of pump chirp can lead to single-photon chirp, depending on the type of spectral correlations in the SPDC photon pairs. In order to make this more evident, we can write the numerator of equation (26) proportional to $\beta\tau_i(\tau_s - \tau_i)$. As discussed in [16], a factorable state with an elongated joint spectrum is possible if $\tau_s = 0$ or $\tau_i = 0$. Thus, interestingly, a factorable, spectrally elongated state with $\tau_i = 0$ is such that the signal-mode single photons remain unchirped despite an arbitrary level of pump chirp. Likewise a state with spectral anti-correlations, characterized by $\tau_s = \tau_i$ which, as discussed in the previous paragraph leads to $\mathscr{C} \to 0$, is also such that the signal-mode single photons remain unchirped despite an arbitrary level of pump chirp (in this case, equation (26) should be evaluated in the limit where $X_{si} \to X_{ss} = X_{ii}$). In general, for other types of joint spectra, the single photons become increasingly chirped as the level of pump chirp is increased.

We are interested in studying how certain key photon-pair properties determine the resulting single-photon properties.
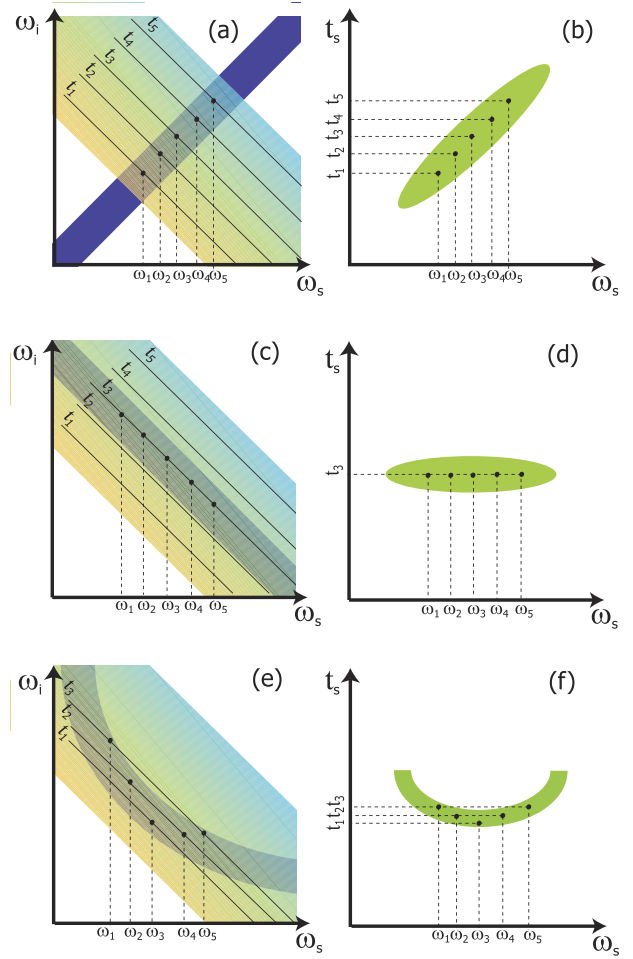
Figure 1. Panels (a), (c) and (e) show schematically how the joint spectrum $|f(\omega_s, \omega_i)|^2$ is determined by the phasematching function $|\phi(\omega_s, \omega_i)|^2$ and the pump envelope function $|\alpha(\omega_s + \omega_i)|^2$. These three panels correspond to: (a) positive correlations, (c) anti-correlations with curvature suppressed and (e) anti-correlations. Panels (b), (d) and (f) show the corresponding inferred single-photon chronocyclic structure.

In particular, we will consider the following two photon-pair properties: (i) type of spectral correlations present as determined by the joint spectrum $|f(\omega_s, \omega_i)|^2$ and (ii) level of quadratic pump chirp present, quantified through the parameter β. In turn, we are particularly interested in studying through the single-photon density matrix and the CWF the single-photon purity and the type of resulting chirp in the single photons. We will consider five representative types of two-photon state, as characterized by the type of spectral correlations present: (i) spectral anti-correlations, (ii) spectral positive correlations, (iii) factorable state with a vertically oriented joint spectrum, (iv) factorable state with a horizontally oriented joint spectrum and (iv) factorable state with a symmetric joint spectrum.

Let us consider each of these types of two-photon states, in turn. Figures 1 and 2 show schematically for these states how the joint spectrum is determined by the functions $\phi(\omega_s, \omega_i)$ and $\alpha(\omega_s + \omega_i)$. These figures also show schematically how quadratic pump chirp, together with
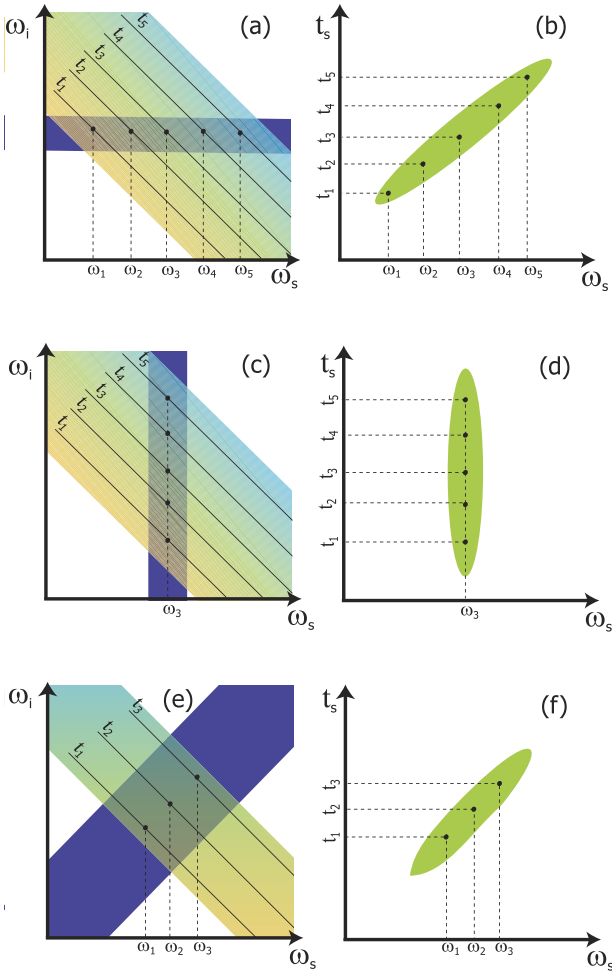
Figure 2. Panels (a), (c) and (e) show schematically how the joint spectrum $|f(\omega_s, \omega_i)|^2$ is determined by the phasematching function $|\phi(\omega_s, \omega_i)|^2$ and the pump envelope function $|\alpha(\omega_s + \omega_i)|^2$. These three panels correspond to: (a) factorable state with horizontally oriented joint spectrum, (c) factorable state with vertically oriented joint spectrum and (e) factorable state with circular-shaped joint spectrum. Panels (b), (d) and (f) show the corresponding inferred single-photon chronocyclic structure.

the unchirped joint spectrum, determine the chronocyclic structure of the single photons which constitute each of the photon pairs. In figure 1 each of the three rows correspond to the following states: positively correlated state, anti-correlated state and a version of the anti-correlated state exhibiting some curvature in the joint spectrum. In each row, the left-hand panel corresponds to a representation of the joint spectrum, with the blue band representing the phasematching function $\phi(\omega_s, \omega_i)$ and the gradient-colored band indicating the pump envelope function $\alpha(\omega_s, \omega_i)$. Note that the PEF exhibits the same orientation in $\{\omega_s, \omega_i\}$ space for all three states, and in all cases the width indicates the use of a broadband, pulsed pump. However, the PMF shows a different orientation in each of the cases, determined by the specific crystal configuration used, which in part determines the resulting spectral entanglement characteristics.

The color gradient used to shade the PEF indicates the presence of quadratic pump chirp, in which case different pump frequencies correspond to different temporal 'slices' of the temporally broadened pump pulse. Thus, we can think of the chirped pump as composed of a temporal sequence of essentially single-frequency components. Each of these single-frequency components, Ω, corresponds to the locus $\omega_s + \omega_i = \Omega$ in $\{\omega_s, \omega_i\}$ space. In this manner, as time progresses within a given pulse, the pump probes different diagonal slices of the joint spectrum, i.e. the joint spectrum produced at a given pump pulse slice with frequency Ω can be written as $|\phi(\omega_s, \omega_i)\alpha(\omega_s + \omega_i)|^2 \delta(\omega_s + \omega_i - \Omega)$. The presence of chirp means that each Ω occurs at a different time, indicated schematically in figures 1 and 2 by black diagonal lines.

From this information, it is possible to infer the chronocyclic structure of, say, the signal-mode single photon. As time progresses within a given quadratically chirped pump pulse, a different diagonal slice of the joint spectrum is emitted. The signal-mode spectrum emitted at a given time is given by the intersection of the locus $\omega_s + \omega_i = \Omega$ (where Ω is time-dependent) with the unchirped joint spectrum $|\phi(\omega_s, \omega_i)\alpha(\omega_s + \omega_i)|^2$. The right panel on each row of figures 1 and 2 shows the inferred chronocyclic structure of the signal-mode single photon, obtained by plotting the points shown within each joint spectrum (left panels of these figures) in the signal-mode chronocyclic space $\{\omega_s, t_s\}$.

There is clear relationship between the type of photon-pair spectral correlations and the resulting single-photon chronocyclic properties. Let us review each of the types of spectral correlations. For photon pairs with positive correlations, there is a monotonic resulting relationship between the time within the pump pulse and the resulting signal-mode frequency. This results in temporal–spectral correlations in the signal-mode single photon, or in other words the signal-mode single photon becomes chirped. These correlations may be positive for positive β or negative for negative β. In contrast, for vanishing pump chirp the signal-mode single photon is likewise unchirped showing no spectral–temporal correlations.

Let us now turn our attention to spectrally anti-correlated photon pairs. In the idealized case of strict spectral anti-correlations, there is a single pump pulse time, related to a single pump frequency Ω that participates in the SPDC process. Thus, in this case, despite the presence of pump chirp, all signal-mode frequencies correspond to a single time of emission, and thus arbitrarily strong pump chirp does not translate into single-photon chirp. Note that this is consistent with the conclusions reached in terms of our analytical expression for the CWF (see equation (23)); in this case, $\tau_s = \tau_i$ means that $\mathscr{C} \to 0$ despite the presence of pump chirp. In a realistic situation for a broadband pump, the joint spectrum exhibits some curvature related to group velocity dispersion as shown schematically in figure 1(e). In this case, the locus $\omega_s + \omega_i - \Omega = 0$ will intersect the joint spectrum at two distinct areas which approach each other and eventually merge into a single zone, as Ω is reduced. The effect of this is that the curvature which characterizes the joint spectrum translates into a curvature in the single-photon chronocyclic structure, as shown schematically in figure 1(f).

Let us now turn our attention to factorable photon pairs; we will consider three different kinds of factorable states:
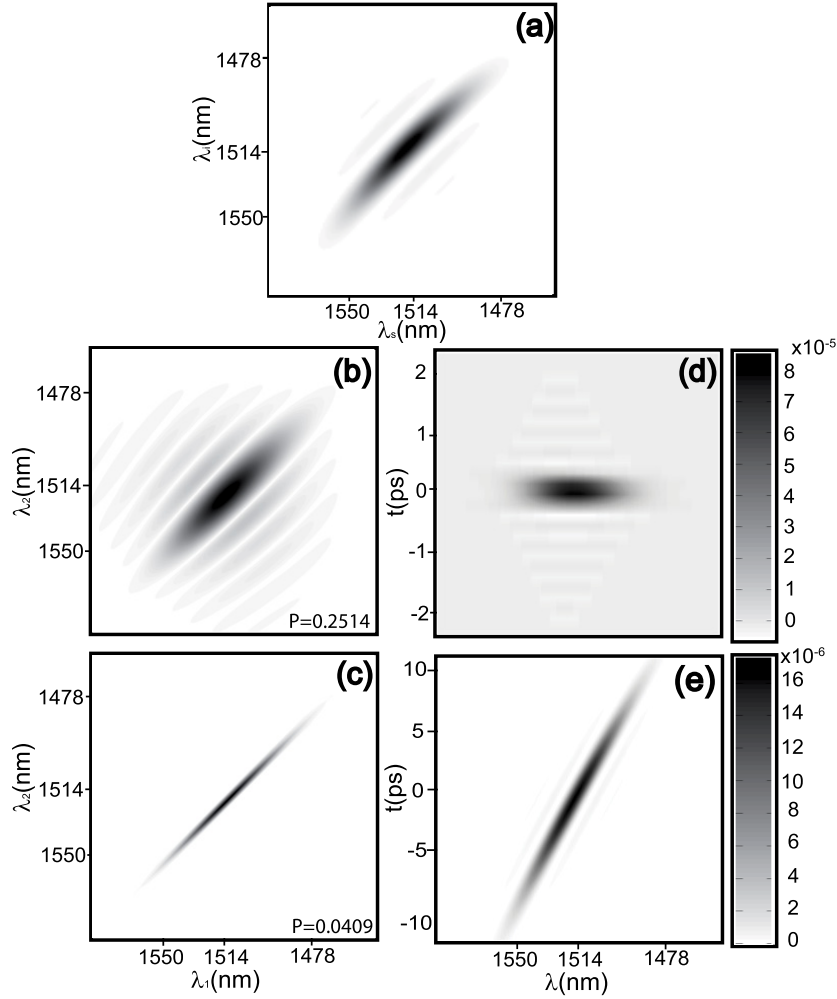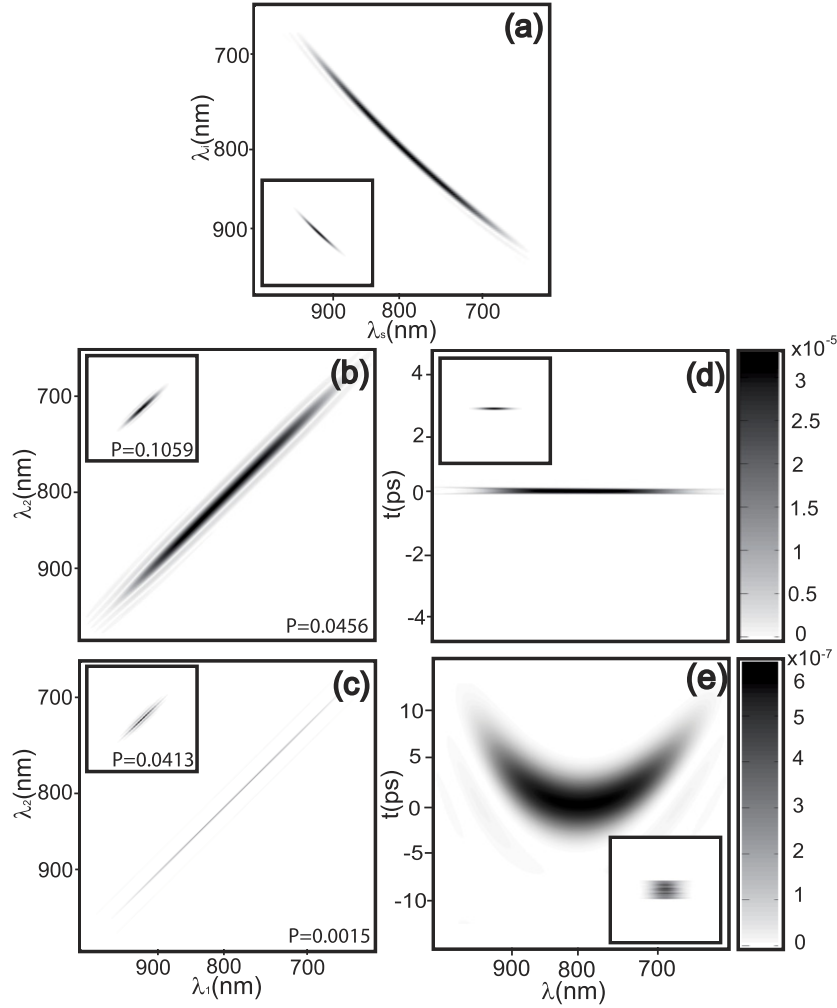
Figure 3. For a state with positive spectral correlations: (a) joint spectrum $|f(\omega_s, \omega_i)|^2$, (b) signal-mode, single-photon density matrix $|\rho_s(\omega_1, \omega_2)|$ with the single-photon purity value indicated, (c) same as (b) but with pump chirp $\beta = 8 \times 10^{-26}$ s^2, (d) single-photon chronocyclic Wigner function $W(\omega, t)$, and (e) same as (d) but with pump chirp $\beta = 8 \times 10^{-26}$ s^2. Note: for convenience, frequency axes are labeled in terms of wavelength.

those with a horizontally oriented joint spectrum, those with a vertically oriented joint spectrum and those with a symmetric joint spectrum. As may be seen from figure 2(a), in the case of a horizontally oriented joint spectrum, the diagonal lines which indicate different pump pulse times intersect the joint spectrum at distinct points. Thus, in this case in a manner qualitatively similar to the positive-correlation case, there is a resulting correlation between the emission time and the signal-mode emission frequency. In the case of a vertically oriented joint spectrum, the situation is different. Here, see figure 2(b), the different emission times of the selected points all correspond to the same signal-mode emission frequency. This implies that the presence of arbitrarily large pump chirp does not result in signal-mode single-photon chirp. Note that this is consistent with the conclusions reached in terms of our analytic expression for the CWF (see equation (23)); in this case, $\tau_i = 0$ means that $\mathscr{C} = 0$ despite the presence of pump chirp.

In what follows, we present specific numerical calculations showing the density matrix, on the one hand, and the chronocyclic Wigner function, on the other hand, for each

type of photon-pair spectral correlations, and also showing the effect of quadratic pump chirp. Note that for these numerical simulations we use the full, unapproximated joint amplitude function. As we will show, the intuition gained both from the joint spectrum schematics (figures 1 and 2) and from the analytical expression of the CWF (see equation (23)) agree well with these numerical results. We will consider a specific implementation for each of the types of source considered above. Table 1 shows for each of these sources: the type of crystal used, the configuration used (type I or type II), the crystal length L, the crystal cut angle θ_{pm}, the crystal phasematching bandwidth $\Delta\omega_c$, the pump center wavelength, λ_o, the pump bandwidth $\Delta\omega$ and the Fourier-transform-limited pulse duration τ. Note that we have used as the definition of $\Delta\omega_c$ the full width at half-maximum of the function $|\phi(\omega/2, \omega/2)|^2$, which may also be thought of as the pump–frequency acceptance function of the crystal.

Photon-pair properties are determined by the characteristics of the crystal and of the pump. In particular, if $\Delta\omega_c < \Delta\omega$, the phasematching function dominates over the pump envelope function to determine the two-photon state, and

Figure 4. For a state with negative spectral correlations: (a) joint spectrum $|f(\omega_s, \omega_i)|^2$, (b) signal-mode, single-photon density matrix $|\rho_s(\omega_1, \omega_2)|$ with the single-photon purity value indicated, (c) same as (b) but with pump chirp $\beta = 8 \times 10^{-26}$ s^2, (d) single-photon chronocyclic Wigner function $W(\omega, t)$, and (e) same as (d) but with pump chirp $\beta = 8 \times 10^{-26}$ s^2. Insets show the result of transmitting the signal and idler photons through a Gaussian-profile spectral filter with 100 nm bandwidth. Note: for convenience, frequency axes are labeled in terms of wavelength.

Table 1. Parameters.

Correlation	Crystal characteristics				Pump		
	Type	L (mm)	θ_{PM} (deg)	$\Delta\omega_c$ (THz)	λ_o (nm)	$\Delta\lambda$ ($\Delta\omega$ (THz))	τ (fs)
Horizontal	KDP-II	5	67.8	15.6	415	5 nm (54.7)	50.7
Vertical	KDP-II	5	67.8	15.6	415	5 nm (54.7)	50.7
Positive	BBO-II	10	28.8	208.2	757	20 nm (65.8)	42.1
Negative	BBO-I	2	29.2	28.3	400	5 nm (58.9)	47.1
Circular	BBO-II	2.293	28.8	328.9	757	15 mm (49.3)	56.2

if $\Delta\omega < \Delta\omega_c$, the pump envelope function dominates over the phase matching function. As may be seen in the table, among the particular states chosen for illustration purposes, for those characterized by an anti-correlated, horizontal and vertical joint spectrum, $\Delta\omega_c < \Delta\omega$, whereas for the positive-correlation and the factorable with a circular joint spectrum states, $\Delta\omega_c > \Delta\omega$.

In all sources considered here, see table 1, we assume frequency-degenerate, collinear SPDC. Likewise, in all cases

involving non-zero pump chirp, we have assumed a value of $\beta = 8 \times 10^{-26}$ s^2.

Figure 3 corresponds to the state with positive correlations; panel (a) shows the joint spectrum. The entanglement present implies that the signal-mode single photons are impure, as indicated by the diagonal structure of the density matrix; panel (b) is a plot of $|\rho_s(\omega_1, \omega_2)|$, for $\beta = 0$. The presence of pump chirp further reduces the width along the anti-diagonal, i.e. ω', direction of the
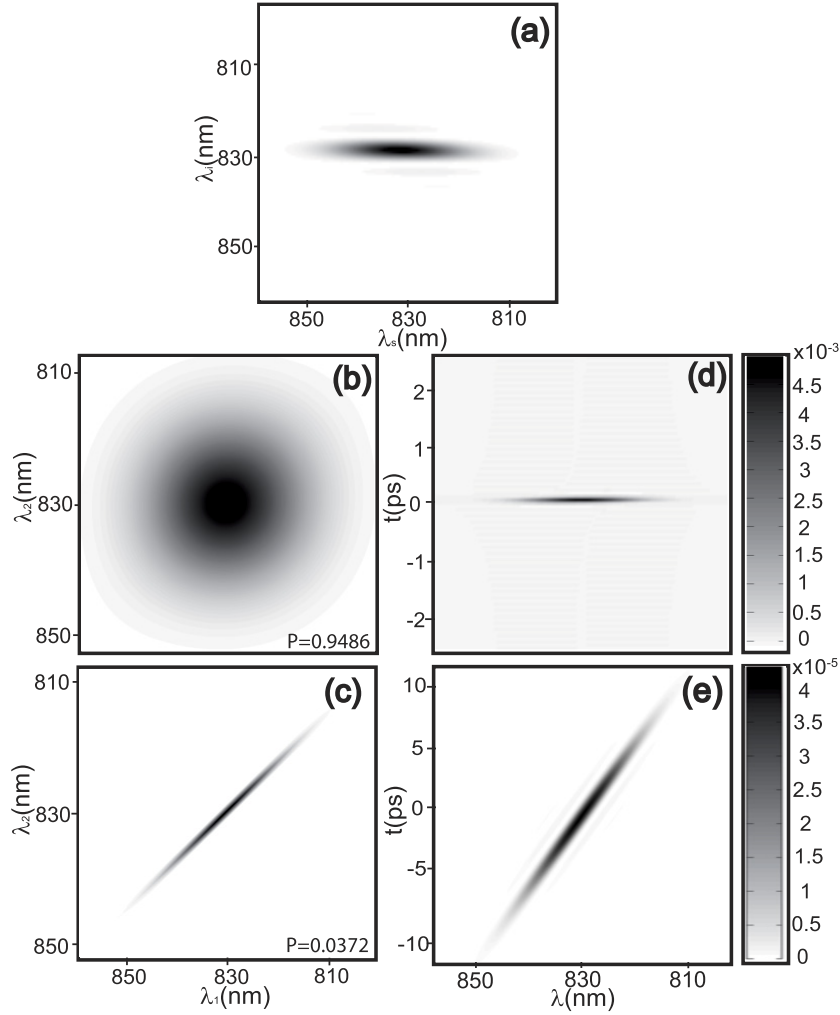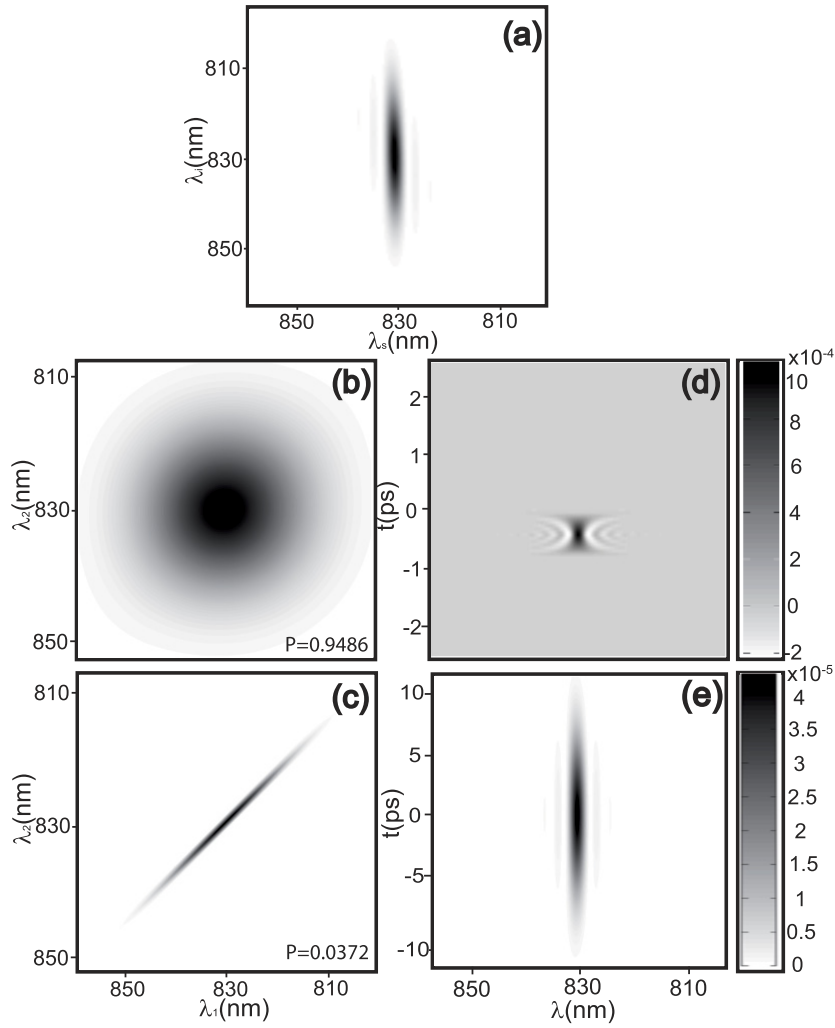
Figure 5. For a factorable state with a horizontally oriented joint spectrum: (a) joint spectrum $|f(\omega_s, \omega_i)|^2$, (b) signal-mode, single-photon density matrix $|\rho_s(\omega_1, \omega_2)|$ with the single-photon purity value indicated, (c) same as (b) but with pump chirp $\beta = 8 \times 10^{-26}$ s^2, (d) single-photon chronocyclic Wigner function $W(\omega, t)$, and (e) same as (d) but with pump chirp $\beta = 8 \times 10^{-26}$ s^2. Note: for convenience, frequency axes are labeled in terms of wavelength.

density matrix, as discussed above due to averaging, see panel (c). In the absence of pump chirp, signal-mode single photons are unchirped, i.e. emission times and frequencies are uncorrelated, as is clear from the CWF plotted in panel (d). The presence of pump chirp, as discussed above for this state, has the effect of chirping the signal-mode single photon, as is clear from the time–frequency correlations in the CWF plotted in the presence of chirp, see panel (e).

Figure 4 corresponds to the spectrally anti-correlated state; panel (a) shows the joint spectrum. Note that the joint spectrum exhibits some curvature in the $\{\omega_s, \omega_i\}$ space, related to group velocity dispersion of the SPDC photon pair. The emission bandwidth, i.e. the width of the SPS, of 0.23 μm is considerable. The inset of panel (a) shows the joint spectrum assuming that the signal and idler photons are each transmitted through a Gaussian-profile bandpass filter with 100 nm bandwidth; as can be appreciated, the curvature is then essentially suppressed. As in the case of positive correlations, the entanglement present implies that the signal-mode single photons are impure as indicated by

the diagonal structure of the density matrix; panel (b) is a plot of $|\rho_s(\omega_1, \omega_2)|$, for $\beta = 0$. Again, the presence of pump chirp further reduces the width along the anti-diagonal of the density matrix due to averaging, see panel (c). As for the positively correlated case, in the absence of chirp, the signal-mode single photons are unchirped, i.e. emission times and frequencies are uncorrelated, as is clear from the CWF plotted in panel (d). As discussed above, the anti-correlated state is relatively insensitive to pump chirp. Let us first consider the filtered state shown in the inset of panel (a). The effect of pump chirp on the CWF for this filtered, anti-correlated state may be seen in the inset of panel (e); it is clear that, despite the presence of pump chirp, there is no resulting chirp in the signal-mode single photons. In the case where spectral filtering is not used, the CWF shows a curvature which, as discussed above, is related to the curvature of the joint spectrum; see panel (e).

Figure 5 corresponds to the factorable state, with a horizontally oriented joint spectrum; panel (a) shows a plot of the joint spectrum. The nearly factorable character of
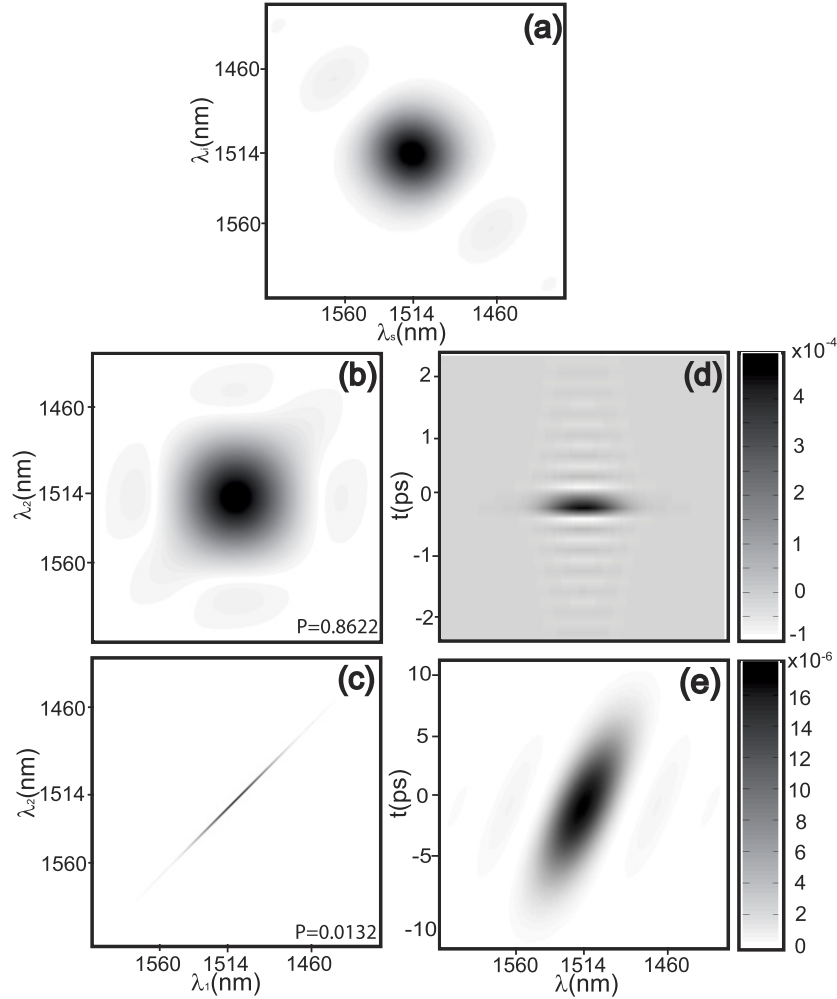
Figure 6. For a factorable state with a vertically oriented joint spectrum: (a) joint spectrum $|f(\omega_s, \omega_i)|^2$, (b) signal-mode, single-photon density matrix $|\rho_s(\omega_1, \omega_2)|$ with the single-photon purity value indicated, (c) same as (b) but with pump chirp $\beta = 8 \times 10^{-26}$ s^2, (d) single-photon chronocyclic Wigner function $W(\omega, t)$, and (e) same as (d) but with pump chirp $\beta = 8 \times 10^{-26}$ s^2. Note: for convenience, frequency axes are labeled in terms of wavelength.

the photon-pair state implies that the signal-mode single photons are basically pure in the absence of pump chirp. This in turn implies that some of the coherences, i.e. the off-diagonal elements of the density matrix are non-zero. This is evident in panel (b), which represents a plot of $|\rho_s(\omega_1, \omega_2)|$. The presence of pump chirp has the expected effect of averaging out the off-diagonal elements, so that the density matrix acquires a diagonal structure, as shown in panel (c). In the absence of pump chirp, signal-mode single photons are unchirped, i.e. emission times and frequencies are uncorrelated, as is clear from the CWF, plotted in panel (d). The presence of pump chirp, as discussed above for this state, has the effect of chirping the signal-mode single photon as is clear from the time–frequency correlations in the CWF plotted for $\beta \neq 0$, see panel (e).

Figure 6 corresponds to the factorable state, with a vertically oriented joint spectrum; panel (a) shows a plot of the joint spectrum. The nearly factorable character of the photon-pair state implies that the signal-mode single photons are basically pure in the absence of pump chirp. As for the

factorable state with a horizontally oriented joint spectrum, this in turn implies that some of the coherences, i.e. the off-diagonal elements of the density matrix, are non-zero. This is evident in panel (b), which represents a plot of $|\rho_s(\omega_1, \omega_2)|$. The presence of pump chirp has the expected effect of averaging out the off-diagonal elements, so that the density matrix acquires a diagonal structure, as shown in panel (c). In the absence of pump chirp, signal-mode single photons are unchirped, i.e. emission times and frequencies are uncorrelated, as is clear from the CWF, plotted in panel (d). As discussed above, this state has the property that, despite the presence of pump chirp, the signal-mode single photons remain basically unchirped, as is evident from the CWF with $\beta \neq 0$, plotted in panel (e).

Finally, figure 7 corresponds to the factorable state, with a symmetric, or circularly shaped, joint spectrum; panel (a) shows a plot of the joint spectrum. The nearly factorable character of the photon-pair state implies that the signal-mode single photons are basically pure in the absence of pump chirp. As for the previous two types of factorable states above, this

Figure 7. For a factorable state with a circular-shaped joint spectrum: (a) joint spectrum $|f(\omega_s, \omega_i)|^2$, (b) signal-mode, single-photon density matrix $|\rho_s(\omega_1, \omega_2)|$ with the single-photon purity value indicated, (c) same as (b) but with pump chirp $\beta = 8 \times 10^{-26} \text{ s}^2$, (d) single-photon chronocyclic Wigner function $W(\omega, t)$, and (e) same as (d) but with pump chirp $\beta = 8 \times 10^{-26} \text{ s}^2$. Note: for convenience, frequency axes are labeled in terms of wavelength.

in turn implies that for $\beta = 0$ some of the coherences, i.e. the off-diagonal elements of the density matrix, are non-zero. This is evident in panel (b), which represents a plot of $|\rho_s(\omega_1, \omega_2)|$. The presence of pump chirp has the expected effect of averaging out the off-diagonal elements, so that the density matrix acquires a diagonal structure, as shown in panel (c). In the absence of pump chirp, signal-mode single photons are unchirped, i.e. emission times and frequencies are uncorrelated, as is clear from the CWF, plotted in panel (d). In the presence of pump chirp, the signal-mode single photons acquire a chirp as is evident from the CWF with $\beta \neq 0$, plotted in panel (e).

3. Conclusions

In this paper we have studied the chronocyclic properties of the single-photon constituents of photon pairs generated by the process of spontaneous parametric downconversion. We have studied how photon-pair properties, in particular (i) the type of signal–idler spectral correlations and (ii) pump

chirp, determine the resulting single-photon properties, in particular the purity and the single-photon chirp. We have studied single-photon properties through the corresponding single-photon spectral density matrix $\rho_s(\omega_1, \omega_2)$, and in chronocyclic space through the single-photon chronocyclic Wigner function $W(\omega, t)$, and how these are determined by photon-pair properties, including the joint spectrum $|f(\omega_s, \omega_i)|^2$ and the level of pump chirp β. We have studied the relationship between these functions and the first degree of spectral coherence $S(\omega_1, \omega_2)$, on the one hand, and the first degree of temporal coherence $\Gamma(t_1, t_2)$, on the other hand.

As we have shown before, pump chirp may be used as an effective tool to control photon-pair entanglement, or equivalently to control the single-photon purity. Varying the level of pump chirp in order to control spectral entanglement also results in a modified chronocyclic single-photon character. In this paper we focus on the study of this single-photon chronocyclic character, in particular the single-photon chirp, and how this is determined by photon-pair properties. We find that, besides the previously understood link between pump chirp and degree of photon-pair entanglement or single-

photon purity, pump chirp in general leads to single-photon chirp, in a manner determined by the type of spectral correlations present. In fact, for certain types of signal–idler spectral correlations single photons remain unchirped despite the presence of pump chirp. We hope that this paper will contribute to a better appreciation of the multi-mode, spectral and temporal, character of single photons derived from spontaneous parametric downconversion.

Acknowledgments

References

[1] Kwiat P G, Mattle K, Weinfurter H, Zeilinger A, Sergienko A V and Shih Y 1995 *Phys. Rev. Lett.* **75** 4337
[2] Kwiat P G, Waks E, White A G, Appelbaum I and Eberhard P H 1999 *Phys. Rev.* A **60** R773–6
[3] Mair A, Vaziri A, Weihs G and Zeilinger A 2001 *Nature* **412** 313
[4] Osorio C I, Valencia A and Torres J P 2008 *New J. Phys.* **10** 113012
[5] Vicent L E, U'Ren A B, Rangarajan R, Osorio C I, Torres J P, Zhang L and Walmsley I A 2010 *New J. Phys.* **12** 093027
[6] Grice W P and Walmsley I A 1997 *Phys. Rev.* A **56** 1627–34
[7] Howell J C, Bennink R S, Bentley S J and Boyd R W 2004 *Phys. Rev. Lett.* **92** 210403
[8] Haase A, Piro N, Eschner J and Mitchell M W 2009 *Opt. Lett.* **34** 55
[9] Mosley P J, Lundeen J S, Smith B J, Wasylczyk P, U'Ren A B, Silberhorn C and Walmsley I A 2008 *Phys. Rev. Lett.* **100** 133601
[10] O'Donnell K A and U'Ren A B 2007 *Opt. Lett.* **32** 817
[11] U'Ren A B, Silberhorn C, Banaszek K and Walmsley I A 2004 *Phys. Rev. Lett.* **93** 093601
[12] Pittan T B, Javobs B C and Franson J D 2005 *Opt. Commun.* **246** 545
[13] Lvovsky A I, Hansen H, Aichele T, Benson O, Mlynek J and Schiller S 2001 *Phys. Rev. Lett.* **87** 050402
[14] Aichele T, Lvovsky A I and Schiller S 2002 *Eur. Phys. J.* D **18** 237
[15] Jeronimo-Moreo Y and U'Ren A B 2009 *Phys. Rev.* A **79** 033839
[16] U'Ren A B, Silberhorn Ch, Erdmann R, Banaszek K, Grice W P, Walmsley I A and Raymer M G 2005 *Laser Phys.* **15** 146
[17] Paye J 1992 *IEEE J. Quantum Electron.* **28** 2262
[18] U'Ren A B, Jeronimo-Moreno Y and García-Gracia H 2007 *Phys. Rev.* A **75** 023810
[19] Torres-Company V, Valencia A and Torres J P 2009 *Opt. Lett.* **34** 1177–9